Received: 14 September 2023 | Revised: 19 December 2023 | Accepted: 21 December 2023

DOI: 10.1002/alz.13693

Alzheimer's & Dementia®
THE JOURNAL OF THE ALZHEIMER'S ASSOCIATION

RESEARCH ARTICLE

Diffusion MRI relates to plasma Aβ42/40 in PET negative participants without dementia

Jesse C. DeSimone[1,2] | Wei-en Wang[1,2] | David A. Loewenstein[2,3,4] | Ranjan Duara[2,5] | Glenn E. Smith[2,6] | Karen N. McFarland[2,7] | Melissa J. Armstrong[2,7,8] | Darren M. Weber[9] | Warren Barker[2,5] | Stephen A. Coombes[1,2,10] | David E. Vaillancourt[1,2,7,8,10]

[1]Department of Applied Physiology and Kinesiology, University of Florida, Gainesville, Florida, USA

[2]1Florida Alzheimer's Disease Research Center, Gainesville, Florida, USA

[3]Center for Cognitive Neuroscience and Aging, University of Miami Miller School of Medicine, Miami, Florida, USA

[4]Department of Psychiatry and Behavioral Sciences, University of Miami Miller School of Medicine, Miami, Florida, USA

[5]Wien Center for Alzheimer's Disease and Memory Disorders, Mount Sinai Medical Center, Miami Beach, Florida, USA

[6]Department of Clinical and Health Psychology, University of Florida, Gainesville, Florida, USA

[7]Department of Neurology, University of Florida, Gainesville, Florida, USA

[8]Norman Fixel Institute for Neurological Diseases, University of Florida, Gainesville, Florida, USA

[9]Quest Diagnostics Nichols Institute, San Juan Capistrano, California, USA

[10]J. Crayton Pruitt Family Department of Biomedical Engineering, University of Florida, Gainesville, Florida, USA

Correspondence
David E. Vaillancourt, PhD, Department of Applied Physiology and Kinesiology, University of Florida, PO Box 118205, Gainesville, FL 32611-8205, USA.
Email: vcourt@ufl.edu

Funding information
National Institutes of Health, Grant/Award Numbers: P30AG066506, T32NS082168

Abstract

INTRODUCTION: Magnetic resonance imaging (MRI) biomarkers are needed for indexing early biological stages of Alzheimer's disease (AD), such as plasma amyloid-β (Aβ42/40) positivity in Aβ positron emission tomography (PET) negative individuals.

METHODS: Diffusion free-water (FW) MRI was acquired in individuals with normal cognition (NC) and mild cognitive impairment (MCI) with Aβ plasma-/PET- (NC = 22, MCI = 60), plasma+/PET- (NC = 5, MCI = 20), and plasma+/PET+ (AD dementia = 21) biomarker status. Gray and white matter FW and fractional anisotropy (FAt) were compared cross-sectionally and the relationships between imaging, plasma and PET biomarkers were assessed.

RESULTS: Plasma+/PET- demonstrated increased FW (24 regions) and decreased FAt (66 regions) compared to plasma-/PET-. FW (16 regions) and FAt (51 regions) were increased in plasma+/PET+ compared to plasma+/PET-. Composite brain FW correlated with plasma Aβ42/40 and p-tau181.

DISCUSSION: FW imaging changes distinguish plasma Aβ42/40 positive and negative groups, independent of group differences in cognitive status, Aβ PET status, and other

plasma biomarkers (i.e., t-tau, p-tau181, glial fibrillary acidic protein, neurofilament light).

KEYWORDS
Alzheimer's disease, amyloid, biomarker, diffusion, free-water, magnetic resonance imaging

Highlights

- Plasma Aβ42/40 positivity is associated with brain microstructure decline.
- Plasma+/PET- demonstrated increased FW in 24 total GM and WM regions.
- Plasma+/PET- demonstrated decreased FAt in 66 total GM and WM regions.
- Whole-brain FW correlated with plasma Aβ42/40 and p-tau181 measures.
- Plasma+/PET- demonstrated decreased cortical volume and thickness.

1 | BACKGROUND

Amyloid-β (Aβ) pathology is a hallmark of Alzheimer's disease (AD) and commonly regarded as the earliest preclinical indicator.[1,2] In vivo detection of Aβ can be achieved using fluid biomarkers such as reduced (i.e., positive) Aβ42/40 ratio in plasma and positron emission tomography (PET) imaging of cerebral Aβ deposition in the brain. Plasma Aβ42/40 has emerged as a surrogate index for measuring brain amyloidosis and may have important implications for screening and detection of individuals at risk of AD and dementia. Several studies have now shown that plasma Aβ42/40 by high-precision mass spectrometry predicts Aβ PET status with high area-under-the-curve (AUC; range: 0.78–0.88).[3–8]

One emerging hypothesis is that a positive plasma Aβ42/40 test in Aβ PET negative individuals could indicate an early stage of brain amyloidosis and represent a biological risk factor for AD.[4,9,10] Individuals with isolated plasma Aβ42/40 positivity (plasma+/PET-) at baseline were found to have a 15-fold higher risk for converting to Aβ PET positive at follow-up compared to those with concordant negative plasma Aβ42/40 and Aβ PET (plasma-/PET-).[4] Lower baseline plasma Aβ42/40 has been associated longitudinally with increased brain Aβ accumulation,[11] cognitive decline,[12] and dementia risk.[13] Developing in vivo neuroimaging biomarkers that are sensitive to isolated plasma Aβ42/40 positivity is important because it would enable better understanding of early disease pathophysiology and foster new approaches to early diagnosis and monitoring of progression.

Diffusion magnetic resonance imaging (MRI) has emerged as a reliable and noninvasive tool for in vivo detection and monitoring of neurodegenerative changes in the brain.[14–16] An advanced diffusion postprocessing technique called free-water (FW) imaging uses a two-compartment model to separate extracellular and tissue-specific diffusion properties.[17] The approach incorporates a tissue-based operator for modeling isotropic and anisotropic tensors and is advantageous for measuring gray (GM) and white matter (WM) microstructure.[18,19] The model quantifies the fractional volume of isotropic FW, which is principally found in the extracellular environment. The FW contribution is then eliminated and the residual diffusion signal is used to determine fractional anisotropy specific to tissue compartment (FAt).[17,20] Increased FW is sensitive to reduced tissue compartment volume and inflammation surrounding brain parenchyma.[17,19,21,22] Reduced FAt relates to axonal demyelination and degeneration, while inflammation and glial scarring surrounding tissue can lead to increased anisotropy.[16,23–25]

Microstructural decline of WM and GM is a common finding in neurodegenerative conditions, including AD,[26] Parkinson's disease,[15] and aging.[27] Increased FW of widespread WM tracts has been reported in mild cognitive impairment (MCI) and AD compared to control brains.[28–30] Increased FW and decreased FAt values in medial temporal WM tracts at baseline were found to associate with more rapid longitudinal cognitive decline.[31] FW changes in hippocampus, entorhinal cortex, and nucleus basalis of Meynert are sensitive to early stages MCI,[26,32] and cortical FW was a strong predictor of longitudinal cognitive decline in MCI.[33] It is unknown, however, whether unique FW or FAt patterns characterize individuals with isolated plasma Aβ42/40 positivity compared to those with normal plasma and PET Aβ status. Such a finding would suggest that FW imaging can be leveraged for evaluating pathophysiology during the earliest biological stages of AD.

This study enrolled participants with normal cognition (NC) and mild cognitive impairment (MCI) with plasma Aβ42/40 negative/PET negative (plasma-/PET-) and Aβ42/40 positive/PET negative (plasma+/PET-) status, as well as AD dementia participants with Aβ42/40 positive/PET positive (plasma+/PET+) status. FW and FAt were computed across 136 total GM regions and WM tracts and compared cross-sectionally between groups. We tested the primary hypothesis that isolated plasma Aβ42/40 positivity in the plasma+/PET- group associates with increased FW and decreased FAt in the brain compared to the plasma-/PET- group. We also assessed

whether FW and FAt related to other plasma biomarkers, including total tau (t-tau), phosphorylated tau181 (p-tau181), neurofilament light (NfL), and glial fibrillary acidic protein (GFAP).

RESEARCH IN CONTEXT

1. **Systematic review**: A review using available public databases yielded no evidence that diffusion free-water (FW) magnetic resonance imaging (MRI) has been used to assess in vivo brain microstructure changes associated with plasma amyloid-β (Aβ42/40) positivity in amyloid positron emission tomography (PET) negative research participants without dementia.
2. **Interpretation**: FW imaging changes distinguish plasma Aβ42/40 positive and negative groups. Plasma Aβ42/40 positivity associates with increased extracellular FW and decreased tissue FAt compared to those with normal plasma and PET Aβ status. FW imaging is sensitive to brain microstructure decline even when even when brain Aβ PET reactivity is not adequate to achieve positivity thresholds.
3. **Future directions**: FW imaging may provide noninvasive readouts for monitoring early changes in AD pathophysiology. Future longitudinal studies are critical for validating FW imaging as a tool for predicting and measuring disease progression.

2 | METHODS

2.1 | Participants and data collection

Diffusion MRI data were acquired in 128 research participants from the 1Florida Alzheimer's Disease Research Center (ADRC). Two study cohorts were included: an Aβ PET negative cohort of 107 participants without dementia (NC: n = 27; MCI: n = 80) and an Aβ PET positive cohort of 21 participants with AD dementia. Cognitive status was determined using the 1Florida ADRC diagnostic algorithm as previously described.[34] Demographic, cognitive, and biomarker measures were collected in all participants. The cognitive battery included Clinical Dementia Rating-Sum of Boxes (CDR-SB),[35] Hopkins Verbal Learning Test – Revised (HVLT-R),[36] and neuropsychological measures of the National Alzheimer's Coordinating Center Uniform Data Set (NACC-UDS).[37] The plasma biomarker panel included: Aβ42, Aβ40, Aβ42/40 ratio, t-tau, p-tau181, NfL, and GFAP. Demographic, cognitive, and biomarker data are provided in Table 1.

2.2 | Plasma biomarker quantification methods

Blood samples were centrifuged immediately after draw and stored at −80°C. Plasma Aβ42/40 was determined by the Quest AD-Detect, beta–amyloid 42/40 ratio, plasma test (Quest Diagnostics, San Juan Capistrano, CA; test code: 11786), which uses high-throughput liquid chromatography/tandem mass spectrometry (LC-MS/MS). MS-based approaches have yielded improved classification between Aβ PET negative and positive participants compared to immunoassays.[6] An initial clinical validation study of the Quest AD-Detect plasma test demonstrated high AUC for differentiating Aβ PET positive from PET negative individuals[38] and comparable performance to other validated MS-based assays.[3–6] Other plasma biomarkers, including t-tau (N3PA Advantage Kit, Item #101995), p-tau181 (pTau-181 Advantage V2 kit, Item #103714), NfL and GFAP (Neurology 2-Plex B kit, Item #103520), were analyzed using single-molecule array immunoassays (Quanterix Corporation, Lexington, MA).[39]

2.3 | Amyloid PET imaging

PET scans with [^{18}F]florbetaben or [^{18}F]florbetapir tracers were acquired in all participants using a Siemens 16 Biograph PET/CT scanner according to previously described methods.[40] Following image reconstruction, global amyloid status (+/-) was determined based on visual inspection by an experienced rater (R.D.). In studies blinded to diagnosis and cognitive status, R.D. and an independent, trained neurologist have obtained high inter-rater reliability.[40,41] Global cortical-to-cerebellar standardized uptake value ratios (SUVR) were calculated and transformed to Centiloid units for quantitative comparison.[42]

2.4 | Plasma/PET status and group stratification

A receiver operating characteristic (ROC) analysis was used to assess the concordance between plasma Aβ42/40 and Aβ PET status and define the threshold for plasma Aβ42/40 positivity, as done in previous studies.[3–5] Youden index, calculated as max(sensitivity + specificity - 1),[43] was used to determine the optimal cut-point on the ROC curve at which plasma Aβ42/40 maximized the classification of Aβ PET negative and positive participants (*cutpointr* package in R, version 4.2.2). A plasma Aβ42/40 ratio < 0.160 was considered positive and yielded the maximum Youden index on the ROC curve, with AUC = 0.9 (95% CI = 0.85–0.94), sensitivity = 1.0 (95% CI = 0.97–1.0), specificity = 0.79 (95% CI = 0.71–0.87), and accuracy = 0.82 (95% CI = 0.77–0.89) (Figure 1). This level of concordance between MS-based plasma Aβ42/40 and Aβ PET status is comparable to other studies.[3–6] Participants in the Aβ PET negative cohort were stratified, independent of cognitive status (NC, MCI), into Aβ42/40 negative/PET negative (plasma-/PET-, n = 82) and Aβ42/40 positive/PET negative (plasma+/PET-, n = 25) groups. All participants in the Aβ PET positive cohort (n = 21) were found to have a concordant positive plasma Aβ42/40 test (plasma+/PET+) (Table 1).

TABLE 1 Participant demographic, cognitive, and biomarker characteristics.

	(A) Aβ PET negative			(B) Aβ PET positive		
Parameter	Plasma-/ PET-	Plasma+/ PET-	*p*	Plasma+/ PET+	vs plasma-/ PET- *p*	vs plasma+/ PET- *p*
N	82	25	–	21	–	–
Age, y	71.1 (7.5)	74.7 (7.6)	0.197	70.8 (8.8)	0.886	0.162
Sex (M/F), *n*	35/47	11/14	0.907	11/10	0.464	0.653
Education, y	15.8 (3.3)	15.2 (3.5)	0.702	14.2 (3.4)	0.080	0.495
APOE ε4 (0/1+), *n*	65/15	16/9	0.197	12/9	0.023*	0.693
Cognitive status, NC/MCI/dementia	22/60/0	5/20/00	0.702	0/0/21	–	–
CDR-SB	0.9 (1.1)	1.4 (1.1)	0.197	7.2 (3.6)	0.0003*	0.0005*
HVLT-R Total	21.8 (5.9)	19.5 (5.8)	0.230	10.8 (4.4)	0.0003*	0.0005*
HVLT-R Delayed	4.3 (4)	3.7 (4.2)	0.716	0.14 (0.5)	0.0003*	0.0009*
NACC-MoCA	23.8 (3.9)	21.7 (4.7)	0.197	13.6 (4.6)	0.0003*	0.0005*
NACC-LM-Immediate	11.6 (3.5)	10.1 (5.1)	0.230	3.6 (2.7)	0.0003*	0.0005*
NACC-LM-Delayed	10.1 (4)	8.4 (4.4)	0.199	1.1 (2.3)	0.0003*	0.0005*
NACC-CAT-ANIM	18 (5.1)	16.9 (6.3)	0.625	10.7 (4.5)	0.0003*	0.002*
NACC-CAT-VEG	11.3 (4.3)	10.8 (4.8)	0.742	5.5 (3.6)	0.0003*	0.0005*
NACC-VERB-F	12.7 (4.3)	12.1 (4.1)	0.716	10.2 (3.1)	0.021*	0.162
NACC-TRAIL-A	47.1 (22)	58.1 (27.5)	0.197	90.7 (33.1)	0.0003*	0.002*
NACC-TRAIL-B	111.7 (64.1)	142.2 (75.7)	0.197	269.9 (60.5)	0.0003*	0.0005*
Aβ42, pg/mL	72.7 (16.5)	53.5 (13.8)	0.002*	53.1 (12.5)	0.0003*	0.921
Aβ40, pg/mL	396.7 (72.2)	392.3 (90.7)	0.882	398.8 (76.6)	0.886	0.843
Aβ42/40 ratio	0.18 (0.02)	0.14 (0.02)	0.002*	0.13 (0.02)	0.0003*	0.584
t-tau, pg/mL	3.8 (1.2)	3.9 (1.3)	0.907	4.2 (1.8)	0.405	0.652
p-tau181, pg/mL	1.8 (0.9)	2.0 (0.6)	0.590	3.8 (1.5)	0.0003*	0.0005*
NfL, pg/mL	12.3 (7.4)	15.2 (7.8)	0.230	18.4 (9.0)	0.005*	0.272
GFAP, pg/mL	140.3 (67.7)	165.2 (102.6)	0.363	269.6 (124.2)	0.0003*	0.004*
PET Global SUVR	1.02 (0.09)	1.04 (0.09)	0.702	1.52 (0.24)	0.0003*	0.0005*
PET Centiloid	4.03 (14.5)	5.46 (14.2)	0.742	84.35 (43.9)	0.0003*	0.0005*
PET Status (-/+), *n*	82/0	25/0	–	0/21	–	–

Note: Demographic, cognitive, and biomarker measures for participants in the (A) Aβ PET negative cohort ($n = 107$) and (B) Aβ PET positive cohort ($n = 21$). The Aβ PET negative cohort in Panel A is stratified by plasma Aβ42/40 status (negative: plasma-/PET-, $n = 82$; positive: plasma+/PET-, $n = 25$). All participants in the Aβ PET positive cohort were plasma Aβ42/40 positive. Observation frequencies are provided for categorical variables and mean (SD) values are provided for continuous variables. FDR-corrected *p*-values are provided for nonparametric independent sample permutation tests (continuous variables) and Chi-square tests (categorical variables).

Abbreviations: APOE ε4, apolipoprotein E ε4 allele; Aβ, plasma amyloid-β (42-residue isoform, 40-residue isoform, 42/40 ratio); CDR-SB, Clinical Dementia Rating – Sum of Boxes; GFAP, glial fibrillary acidic protein; HVLT-R, Hopkins Verbal Learning Test-Revised (total and delayed recall); MCI, mild cognitive impairment; NACC, National Alzheimer's Coordinating Center – Uniform Data Set; NACC-CAT, categorical fluency test (animals and vegetables); NACC-LM, logical memory test (immediate and delayed recall); NACC-MoCA, Montreal Cognitive Assessment; NACC-TRAIL, oral trail making test (parts A and B); NACC-VERB-F, verbal fluency phonemic "F" test; NC, normal cognition; NfL, neurofilament light; PET, positron emission tomography; p-tau181, phosphorylated tau 181; SUVR, standardized uptake value ratio; t-tau, total tau.

*significant group effect ($p_{FDR} < 0.05$) for the contrast of interest.

2.5 | MRI acquisition

MRI scans were acquired on a 3T Siemens Magnetom Skyra scanner with a 20-channel head/neck coil. The MRI panel included volumetric T1-weighted and diffusion-weighted MRI scans. T1 scans were acquired using a magnetization-prepared rapid gradient-echo (MPRAGE) sequence with the following parameters: repetition time (TR) = 1380 ms, echo time (TE) = 3.03 ms, slices = 176, gap = 0 mm, resolution = 1 mm isotropic. The diffusion acquisition protocol included an echo planar imaging (EPI) sequence with the following parameters: directions = 64, TR = 9000 ms, TE = 90 ms, slices = 64, gap = 0 mm, resolution = 2 mm isotropic, *b*-value = 1000 s/mm^2, b0 images = 1. Raw

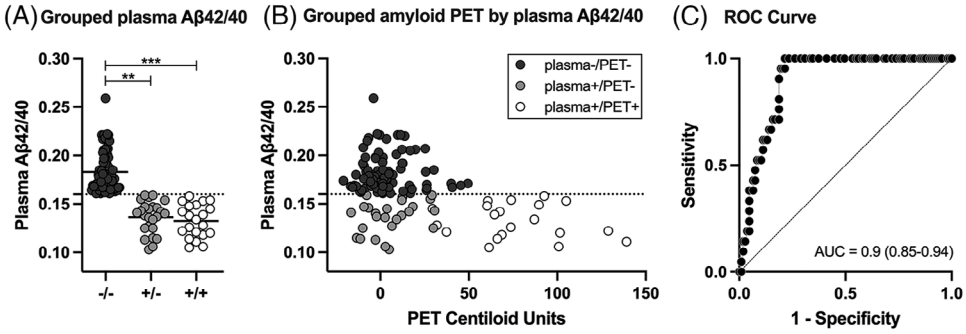

FIGURE 1 Relationship between plasma amyloid-β (Aβ42/40) and Aβ positron emission tomography (PET). (A) Grouped strip plots representing individual plasma Aβ42/40 measurements and groups means (horizontal black lines) in plasma-/PET- (dark gray: -/-), plasma+/PET- (light gray: +/-), and plasma+/PET+ (white: +/+) groups. Statistical denotations for nonparametric independent samples permutation tests: ** $p_{FDR} <= 0.01$, *** $p_{FDR} <= 0.001$. (B) Grouped Aβ PET Centiloid units by plasma Aβ42/40 using the same group color scheme as in plot A. An outlier data point from a single participant in the plasma+/PET+ group was censored for improved visualization but was included in all analyses (PET Centiloid = 230, plasma Aβ42/40 = 0.138). The horizontal dashed lines in plots A and B represent the cut-point for separating plasma Aβ42/40 positive (< 0.16) and negative participants. (C) Receiver operating characteristic (ROC) area-under-the-curve (AUC) showing the correspondence between plasma Aβ42/40 and Aβ PET status (+/-).

T1 and diffusion images were visually inspected and confirmed to be devoid of acquisition artifacts, including incomplete whole-brain coverage, magnetic field inhomogeneities and signal distortions, and overt pathological lesions.

2.6 | MRI processing

2.6.1 | T1 image processing

T1 image processing was performed using an automated reconstruction pipeline in FreeSurfer (version 7.1.0: https://surfer.nmr.mgh.harvard.edu) and included skull stripping, intensity normalization, subcortical segmentation, cortical parcellation, and region-of-interest (ROI) labeling. Cortical volume and thickness measures were calculated in 68 total ROIs (34 bihemispheric) using the Desikan–Killiany atlas.[44] Volumetric-only measures were also calculated in 19 ROIs using the FreeSurfer subcortical segmentation map (five midline, seven bihemispheric). Volumetric measures from each region were divided by estimated total intracranial volume to account for variability in head size.[45] Reconstructed output files were visually inspected to rule out and troubleshoot errors in cortical parcellation and subcortical segmentation prior to analysis.

2.6.2 | Diffusion FW image processing

Diffusion image processing was fully automated using FMRIB Software Library (FSL) (https://fsl.fmrib.ox.ac.uk/fsl/fslwiki), Advanced Normalization Tools (ANTs) (http://stnava.github.io/ANTs/), and custom Linux shell and MATLAB (MathWorks, Natick, MA) scripts. Image distortions due to eddy currents and head motion were corrected using affine transformations and the gradient directions were rotated to account for these corrections. Nonbrain tissue was removed using FSL Brain Extraction Tool. FW and FAt maps were calculated in MATLAB from the corrected diffusion-weighted volumes using a bitensor model.[17] The bitensor model uses a minimization procedure to quantify the fractional volume of FW within each voxel. The predicted signal attenuation due to FW partial volume is then removed to produce a set of corrected tissue-specific diffusion tensors. The corresponding diffusion tensors were used to calculate FAt using FSL DTIFIT. FW and FAt maps were normalized to Montreal Neurological Institute (MNI) space using a nonlinear warping procedure in ANTs. The diffusion pipeline included an automated quality assurance procedure for all data processing steps. Visual inspection was performed on all normalized FW and FAt maps.

FW and FAt were calculated in 136 total ROIs. GM ROIs included 96 regions (two midline, 47 bihemispheric) from the Mayo Clinic Adult Lifespan Template (MCALT; https://www.nitrc.org/projects/mcalt/).[46] Eight additional ROIs (four bihemispheric) comprising the magnocellular cell groups of the basal forebrain were included and derived from a probabilistic mapping study.[47] Basal forebrain ROIs included cell groups within the septum (Ch1-2), horizontal limb of the diagonal band (Ch3), sublenticular nucleus (Ch4; nucleus basalis of Meynert), and posterior portion of the sublenticular nucleus (Ch4p). The anatomical distribution of GM ROIs included frontal/forebrain, temporal, parietal, occipital, limbic, and subcortical parcellations. WM ROIs included 32 tract regions from the Transcallosal Tract Template (TCATT).[28] TCATT includes commissural tracts emerging from 12 prefrontal, 6 frontal, 3 temporal, 5 parietal, and 6 occipital cortical origins and was developed using a high-resolution slice-level postprocessing tractography technique.[28] ROIs were selected based on previous application to AD and MCI studies[28,32,48] and because the combination of different atlases afforded comprehensive coverage of diverse brain regions, tissue types, and microstructural environments.

2.7 | Statistical analysis

2.7.1 | Cross-sectional imaging analysis

Volumetric, thickness, FW, and FAt measures for each ROI were compared cross-sectionally between plasma-/PET-, plasma+/PET-, and plasma+/PET+ groups using a nonparametric permutation analysis of covariance (ANCOVA) model in R (version 4.2.2, *lmperm* library). Volumetric group-level effects were corrected for false discovery rate (FDR) across 87 cortical and subcortical GM ROIs. Cortical thickness group-level effects were FDR-corrected across 64 cortical GM ROIs. FW and FAt group-level effects were FDR-corrected across ROIs, separately for GM (104 tests for both FW and FAt) and WM (32 tests for both FW and FAt). Each model was covaried for age, sex, education, and apolipoprotein E (APOE) $\varepsilon 4$ status and considered significant at $p_{FDR} < 0.05$. Group-level main effects were decomposed posthoc using Tukey's HSD method with family wise error (FWE) correction and considered significant at $p_{FWE} < 0.05$.

2.7.2 | Composite imaging and correlation analysis

A correlation analysis was performed to examine the relationship between diffusion imaging measures (FW, FAt) and other biomarkers, including Aβ42/40, t-tau, p-tau181, NfL, and GFAP in plasma, as well as PET Centiloid units. The average value for each imaging metric (FW, FAt) by tissue type (104 GM ROIs, 32 WM ROIs) combination was calculated for each participant, producing four composite imaging scores (i.e., GM FW, GM FAt, WM FW, WM FAt). Composite imaging scores were compared cross-sectionally using nonparametric permutation ANCOVA models, covaried for age, sex, education, and APOE $\varepsilon 4$ status. Group main effects ($p_{FDR} < 0.05$) were decomposed posthoc using Tukey's HSD method and considered significant at $p_{FWE} < 0.05$. Partial nonparametric Spearman's rank correlations were computed between composite imaging scores and other biomarkers and adjusted for effects of age, sex, education, and APOE $\varepsilon 4$ status. For each composite imaging score, correlation effects were FDR-corrected across all biomarker measures and considered significant at $p_{FDR} < 0.05$.

3 | RESULTS

3.1 | Cross-sectional regional volume and thickness

The ANCOVA model of T1 cortical and subcortical volume yielded significant group effects for 32 of 87 GM ROIs (all $p_{FDR} < 0.05$). The plasma+/PET- group demonstrated significantly reduced volumes compared to plasma-/PET- in 5 of 32 ROIs, including temporal pole, amygdala, and putamen (mean Cohen's $d = -0.65$; all $p_{FWE} < 0.05$). The spatial extent of volumetric decline was greater in the plasma+/PET+ group, with significantly reduced volumes compared to plasma-/PET- in 30 of 32 ROIs (mean Cohen's $d = -0.94$; all $p_{FWE} < 0.05$). This included ROIs across frontal, temporal, parietal, occipital, limbic, and subcortical areas. The plasma+/PET+ group also demonstrated significantly reduced volumes in 16 of 32 ROIs compared to plasma+/PET- (mean Cohen's $d = -0.85$; all $p_{FWE} < 0.05$), including frontal, temporal, parietal, limbic, and subcortical areas. The group means and effects sizes for significant ROI effects are provided in Table S1.

The ANCOVA model of T1 cortical thickness yielded significant group effects for 20 of 68 GM ROIs (all $p_{FDR} < 0.05$). The plasma+/PET- group demonstrated significantly reduced thickness compared to plasma-/PET- in 7 of 20 ROIs (mean Cohen's $d = -0.72$; all $p_{FWE} < 0.05$), including temporal cortex, insula, and fusiform. The plasma+/PET+ group demonstrated significantly reduced T1 thickness compared to plasma-/PET- in all 20 ROIs (mean Cohen's $d = -1.0$; all $p_{FWE} < 0.05$) and in 9 of 20 ROIs compared to plasma+/PET- (mean Cohen's $d = -0.8$; all $p_{FWE} < 0.05$). The effects for both cross-sectional comparisons were largely localized to left and right temporal cortical regions, insula, and entorhinal cortex (Table S2).

3.2 | Cross-sectional regional FW and FAt effects

The ANCOVA model for GM FW yielded significant group effects for 70 of 104 ROIs (all $p_{FDR} < 0.05$) (Figure 2A, Table S3). The plasma+/PET- group demonstrated significantly increased FW compared to plasma-/PET- in 22 of 70 ROIs (mean Cohen's $d = 0.8$; all $p_{FWE} < 0.05$). Key ROIs included hippocampus, basal forebrain (Ch1-2, Ch3), and superior, middle, and inferior temporal regions. FW was also increased in parietal, occipital, and limbic regions. FW in the plasma+/PET+ group was significantly increased compared to plasma-/PET- in 65 of 70 ROIs across frontal, basal forebrain, temporal, parietal, occipital, limbic, and subcortical areas (mean Cohen's $d = 0.82$; all $p_{FWE} < 0.05$). FW was also significantly increased in plasma+/PET+ compared to plasma+/PET- in 11 of 70 ROIs that included hippocampus and Ch4 region of the basal forebrain (nucleus basalis of Meynert) (mean Cohen's $d = 0.53$; all $p_{FWE} < 0.05$).

The ANCOVA model for WM FW yielded significant group effects for 16 of 32 ROIs (all $p_{FDR} < 0.05$) (Figure 2B, Table S4). The plasma+/PET- group demonstrated significantly increased FW compared to plasma-/PET- in 2 of 16 ROIs, including inferior temporal and lingual tracts (mean Cohen's $d = 0.68$; all $p_{FWE} < 0.05$). FW in the plasma+/PET+ group was significantly increased compared to plasma-/PET- in all 16 ROIs, including prefrontal, frontal, temporal, parietal, and occipital tracts (mean Cohen's $d = 0.85$; all $p_{FWE} < 0.05$). FW was also significantly increased in plasma+/PET+ compared to plasma+/PET- in 5 of 16 ROIs that included temporal, parietal, and occipital tracts (mean Cohen's $d = 0.47$; all $p_{FWE} < 0.05$).

The ANCOVA model for GM FAt yielded significant group effects for 50 of 104 GM ROIs (all $p_{FDR} < 0.05$) (Figure 3A, Table S5). The plasma+/PET- group demonstrated significantly reduced FAt compared to plasma-/PET- in 42 of 50 ROIs (mean Cohen's $d = -0.64$; all $p_{FWE} < 0.05$). Several key ROIs included the Ch4p region of the basal forebrain and superior and middle temporal cortex. Other ROIs included parietal, occipital, limbic, and subcortical areas.

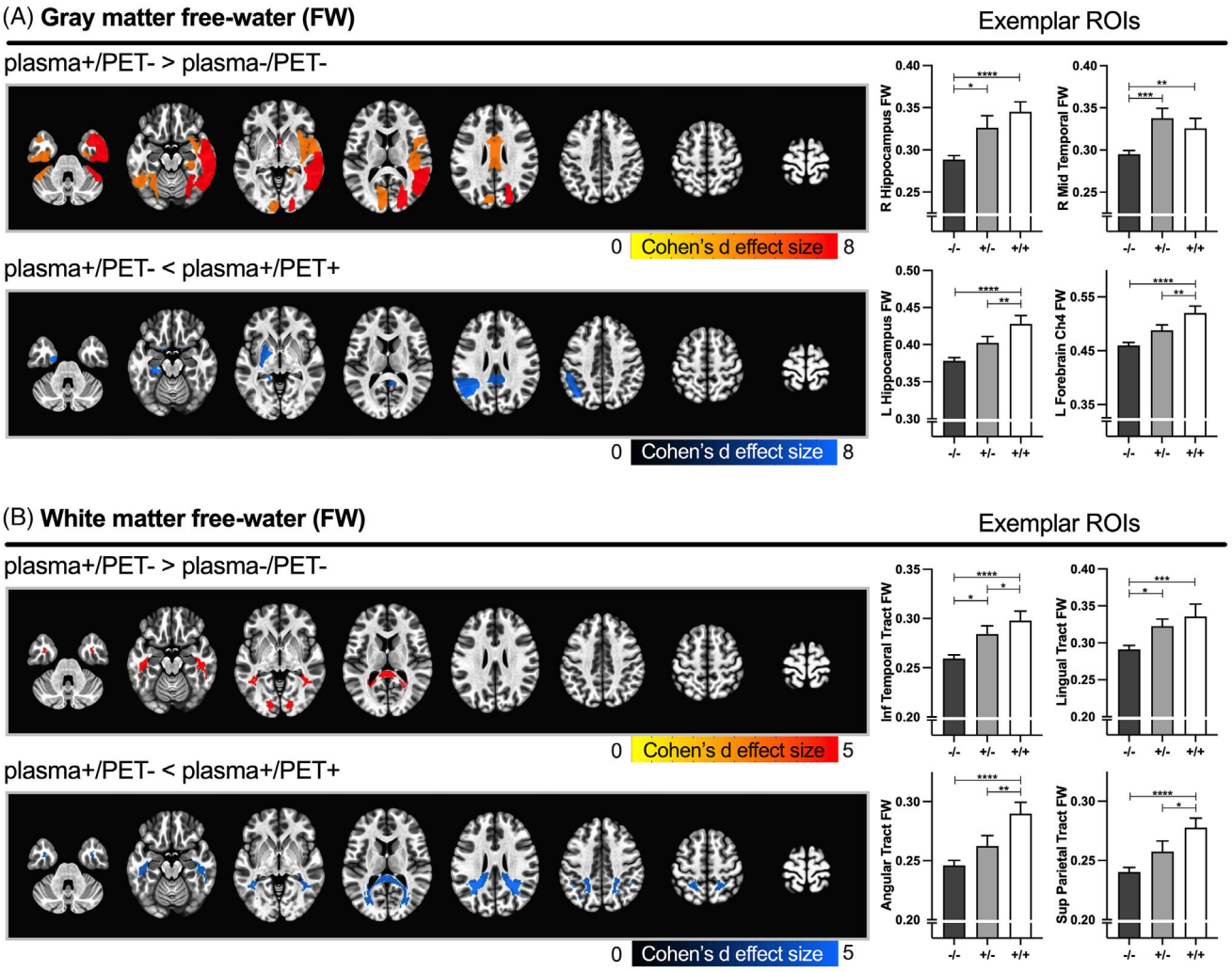

FIGURE 2 Significant free-water (FW) group effects. Spatial maps representing significant FW group effects in gray (A) and white matter (B) regions of interest (ROIs). Red and blue colors represent increased and decreased FW, respectively, for the contrast of interest (* $p_{FWE} < 0.05$). The color scale represents the Cohen's d effect size for the contrast of interest. Exemplar bar plots representing the mean FW values for plasma-/PET- (dark gray: -/-), plasma+/PET- (light gray: +/-), and plasma+/PET+ (white: +/+) groups are provided for select ROIs for each spatial map. Error bars represent the standard error of the mean. Statistical denotations for Tukey contrasts: * $p_{FWE} <= 0.05$, ** $p_{FWE} <= 0.01$, *** $p_{FWE} <= 0.001$, **** $p_{FWE} <= 0.0001$. The significant contrasts for individual gray matter (GM) and white matter (WM) ROIs are provided in Tables S3–4. PET, positron emission tomography.

The plasma+/PET+ group demonstrated significantly increased FAt compared to plasma-/PET- in one ROI in the Ch4p region of the basal forebrain (Cohen's $d = 0.69$, $p_{FWE} = 0.02$). The plasma+/PET+ group also demonstrated significantly increased FAt compared to plasma+/PET- in 38 of 50 ROIs, which included Ch4 region of the basal forebrain, entorhinal cortex, and superior and middle temporal cortex (mean Cohen's $d = 0.96$; all $p_{FWE} < 0.05$).

The ANCOVA model for WM FAt yielded significant group effects for 25 of 32 WM ROIs (all $p_{FDR} < 0.05$) (Figure 3B, Table S6). The plasma+/PET- group demonstrated significantly reduced FAt compared to plasma-/PET- in 23 of 25 ROIs, including prefrontal, frontal, temporal, parietal, and occipital tracts (mean Cohen's $d = -0.73$; all $p_{FWE} < 0.05$). No significant FAt differences were detected between plasma+/PET+ and plasma-/PET-. The plasma+/PET+ group demonstrated significantly increased FAt compared to plasma+/PET- in 13 of 32 ROIs, including prefrontal, frontal, parietal, and temporal tracts (mean Cohen's $d = 0.73$; all $p_{FWE} < 0.05$).

3.3 | Correlation analysis: Composite imaging and plasma biomarkers

The results from the ANCOVA models for composite imaging scores are shown in Figure 4A. As expected, based on the cross-sectional results, significant group effects were uncovered for each composite imaging score (GM FW, GM FAt, WM FW, WM FAt) (all $p_{FDR} < 0.05$). Composite GM FW scores were significantly increased in the plasma+/PET- and plasma+/PET+ groups compared to plasma-/PET- (mean Cohen's $d = 0.81$; all $p_{FWE} < 0.05$), whereas no differences were observed between plasma+/PET- and plasma+/PET+.

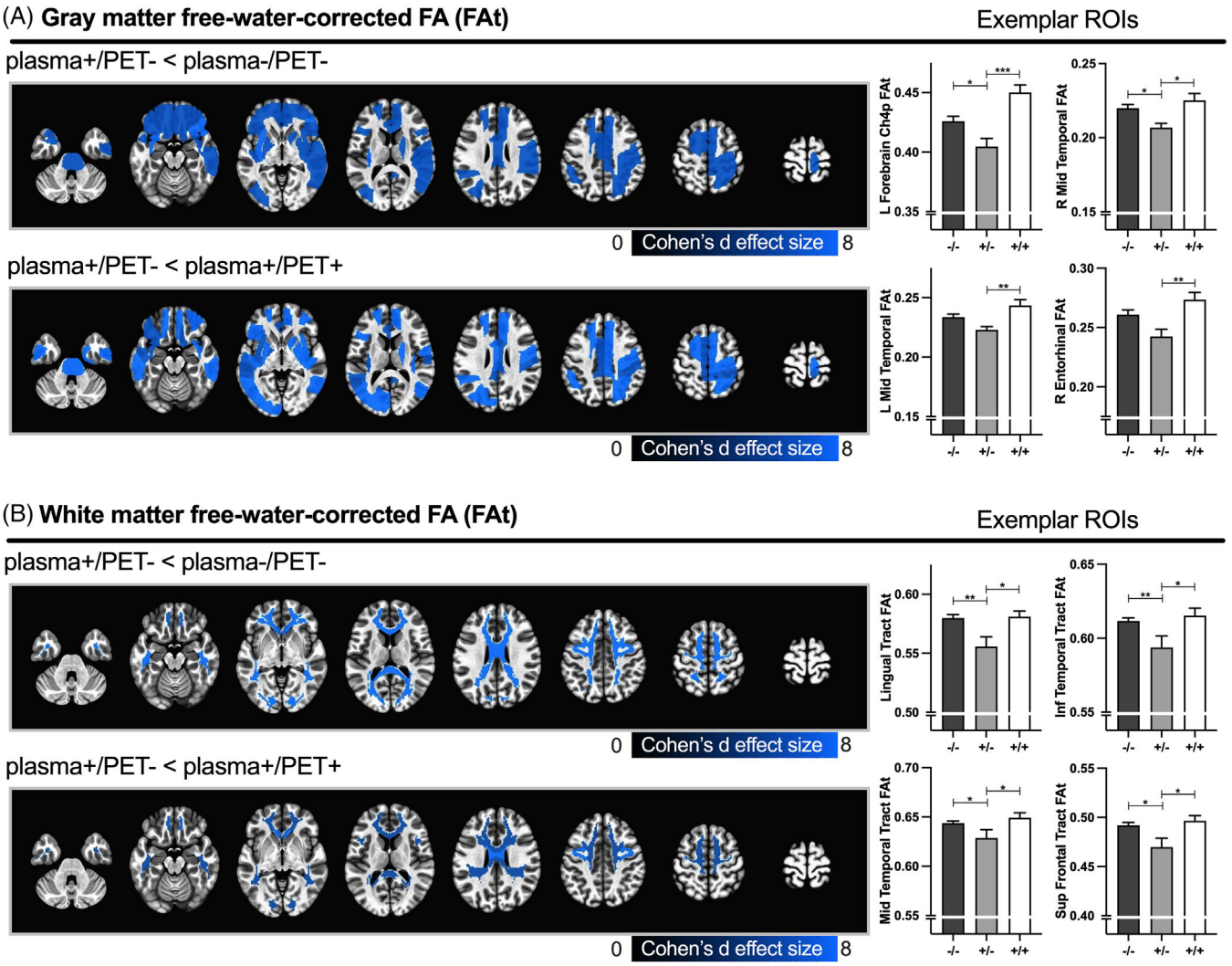

FIGURE 3 Significant free-water-corrected fractional anisotropy (FAt) group effects. Spatial maps representing significant FAt group effects in gray (A) and white matter (B) regions-of-interest (ROIs). Blue colors represent decreased FAt for the contrast of interest (* $p_{FWE} < 0.05$). The color scale represents the Cohen's d effect size for the contrast of interest. Exemplar bar plots representing the mean FAt values for plasma-/PET- (dark gray: -/-), plasma+/PET- (light gray: +/-), and plasma+/PET+ (white: +/+) groups are provided for select ROIs for each spatial map. Error bars represent the standard error of the mean. Statistical denotations for Tukey contrasts: * $p_{FWE} <= 0.05$, ** $p_{FWE} <= 0.01$, *** $p_{FWE} <= 0.001$. The significant contrasts for individual gray matter (GM) and white matter (WM) ROIs are provided in Tables S5–6. PET, positron emission tomography.

Composite WM FW scores were significantly increased in the plasma+/PET+ group compared to plasma-/PET- (Cohen's $d = 0.77$; $p_{FWE} < 0.05$), whereas no differences were observed between plasma+/PET- and plasma-/PET- or between plasma+/PET+ and plasma+/PET- groups. Composite FAt scores in both GM and WM were significantly decreased in the plasma+/PET- group compared to both plasma-/PET- and plasma+/PET+ groups (mean Cohen's $d = -0.83$; all $p_{FWE} < 0.05$), whereas no differences were observed between plasma-/PET- and plasma+/PET+ groups.

In the partial correlation analysis, composite FW scores in GM and WM yielded significant inverse correlations with plasma Aβ42/40 (all $rho < -0.28$; all $p_{FDR} = 0.006$) and positive correlations with p-tau181 (all $rho > 0.35$; all $p_{FDR} < 0.001$) (Figure 4B, Table 2). Composite FW scores in GM and WM were not significantly correlated with t-tau, NfL, GFAP, or PET Centiloid units. The correlation between composite GM FW and plasma NfL approached significance ($rho = 0.22$, $p_{FDR} = 0.05$). Composite FAt scores in GM and WM were not significantly correlated with other biomarkers (Table 2).

4 | DISCUSSION

The primary aim of this study was to evaluate diffusion microstructure changes associated with isolated plasma Aβ42/40 positivity, which has emerged as a potential early biological indicator of AD. A salient finding was that the plasma+/PET- (isolated plasma Aβ42/40 positivity) group demonstrated significantly increased FW and decreased FAt in the brain compared to the plasma-/PET- (normal biomarker) group. In prior studies, FW imaging changes in GM and WM have associated with early stages of MCI in individuals with mixed Aβ

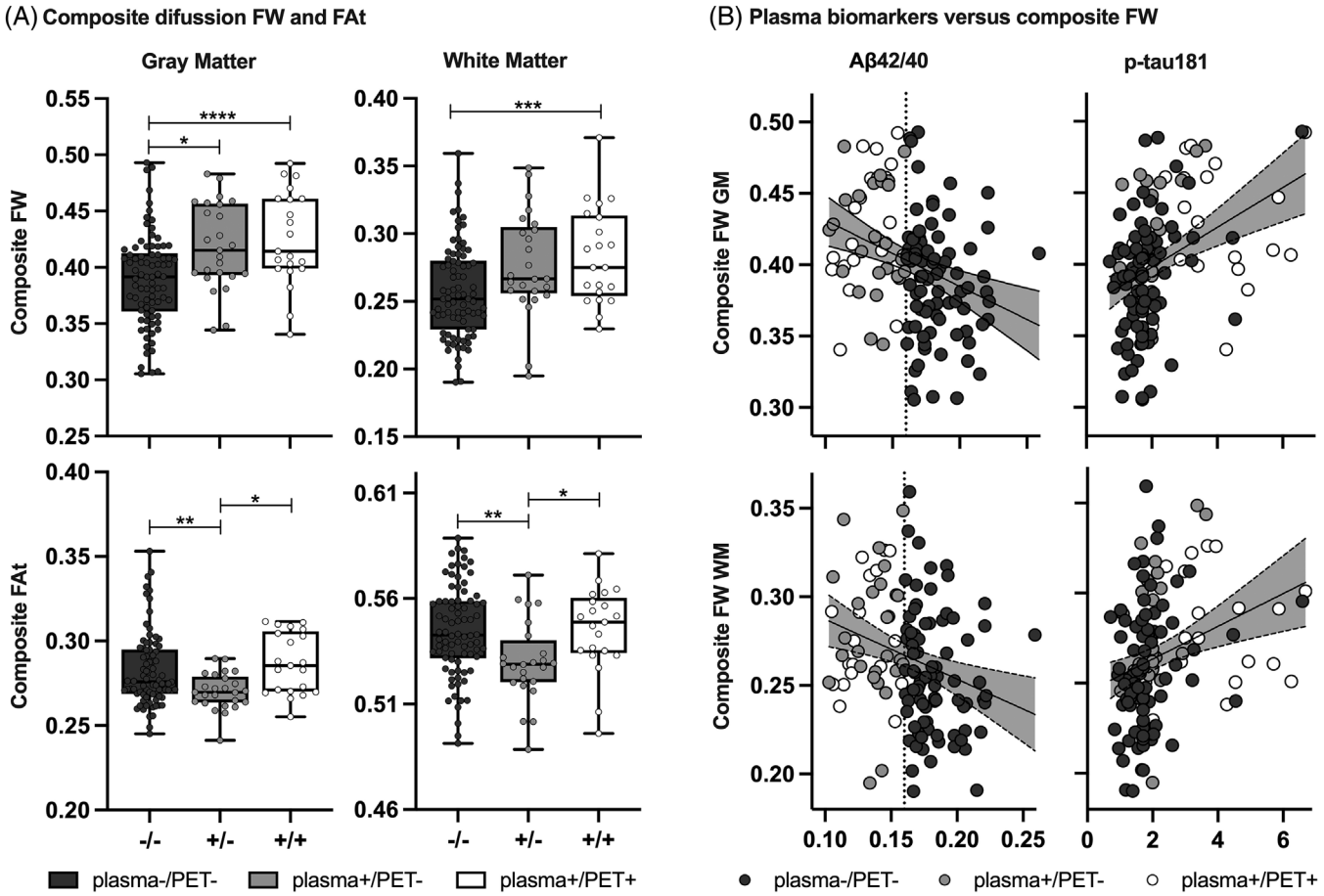

FIGURE 4 Composite imaging scores and correlation plots. (A) Grouped boxplots with overlaid strip plots representing the average (i.e., composite) free-water (FW) (top panel) and FW-corrected fractional anisotropy (FAt) (bottom panel) scores in gray matter (GM) (left panel) and white matter (WM) (right panel) for plasma-/PET- (dark gray: -/-), plasma+/PET- (light gray: +/-), and plasma+/PET+ (white: +/+) groups. Error bars represent the minimum to maximum data points. An outlier composite WM FAt score from a single participant in the plasma+/PET- group was censored for improved visualization but was included in all analyses. Statistical denotations for Tukey contrasts:* $p_{FWE} <= 0.05$, ** $p_{FWE} <= 0.01$, *** $p_{FWE} <= 0.001$, **** $p_{FWE} <= 0.0001$. (B) Grouped correlation plots for composite FW scores in GM (top panel) and WM (bottom panel) with plasma Aβ42/40 (left panel) and p-tau181 (right panel). Individual values are encoded using the same group color scheme as in plot A. Vertical black dashed lines represent the cut-point for separating plasma Aβ42/40 positive (< 0.16) and negative participants, as determined by the receiver operating characteristic (ROC)-Youden analysis. Shaded gray areas represent the 95% confidence interval on the regression estimate (solid black line). PET, positron emission tomography.

PET status.[26,32] The current findings are novel and important in that they indicate that abnormal plasma Aβ42/40 deviations in participants without dementia associates with quantifiable changes in the tissue and extracellular microstructural environments, even when brain Aβ PET reactivity is not adequate to achieve positivity thresholds. FW and FAt changes reflect different biological processes. Increased FW is sensitive to increased neuroinflammation, which affects the partial volume of extracellular environment surrounding brain parenchyma.[19,21] Reduced FAt indicates axonal degeneration and/or demyelination, which affects the organization and diffusion properties of the tissue microstructure.[24]

The inclusion of the plasma+/PET+ group provided an avenue to cross-sectionally examine the relationship between imaging and biological Aβ status. Several key ROIs emerged in the cross-sectional analysis for GM. Compared to the plasma-/PET- group, FW was increased in the plasma+/PET- group in right hippocampus, left and right basal forebrain (Ch1-2 and Ch3), and left and right temporal cortex. In the plasma+/PET+ group, increased FW effects extended to bilateral hippocampus and basal forebrain regions Ch1-2, Ch3, and Ch4 (nucleus basalis of Meynert) compared to the plasma-/PET- group and bilateral Ch4 compared to the plasma+/PET- group. Microstructural decline in these regions has previously been shown in the early stages of MCI, and increased FW has been found to relate to greater cognitive diagnosis severity.[26,32,33] In transcallosal WM tracts (TCATT), the spatial extent of FW effects similarly tracked Aβ status (plasma-/PET- < plasma+/PET- < plasma+/PET+). FW was increased in temporal and occipital tracts in the plasma+/PET- group and extended to prefrontal, frontal, temporal, parietal, and occipital tracts in the plasma+/PET+ group. Previous cross-sectional studies have found that increased FW across widespread WM tracts relates to worsened cognitive

TABLE 2 Correlations between diffusion imaging, plasma, and PET biomarkers.

	Aβ42/40	t-tau	p-tau181	NfL	GFAP	PET Centiloid
FW (GM)	**−0.298 (0.006)***	0.006 (0.95)	**0.385 (< 0.001)***	0.22 (0.05)	0.145 (0.246)	0.11 (0.342)
FW (WM)	**−0.286 (0.006)***	0.054 (0.575)	**0.35 (< 0.001)***	0.174 (0.134)	0.13 (0.287)	0.095 (0.388)
FAt (GM)	0.097 (0.592)	−0.042 (0.809)	−0.038 (0.809)	−0.129 (0.592)	0.002 (0.99)	0.150 (0.529)
FAt (WM)	0.118 (0.430)	−0.021 (0.819)	−0.154 (0.430)	−0.133 (0.430)	−0.035 (0.819)	0.076 (0.585)
Aβ42/40	1	−0.129 (0.17)	**−0.391 (< 0.0001)***	**−0.281 (0.001)***	**−0.228 (0.018)***	**−0.329 (0.001)***
t-tau	–	1	0.188 (0.074)	**0.293 (0.006)***	0.187 (0.074)	0.202 (0.074)
p-tau181	–	–	1	**0.566 (< 0.0001)***	**0.444 (< 0.0001)***	**0.396 (< 0.0001)***
NfL	–	–	–	1	**0.466 (< 0.0001)***	0.186 (0.059)
GFAP	–	–	–	–	1	**0.398 (< 0.0001)***
PET Centiloid	–	–	–	–	–	1

Note: Partial Spearman's rank correlation coefficients (associated FDR-corrected *p*-values) between composite diffusion imaging scores (FW, FAt), plasma biomarkers and Aβ PET Centiloid units, corrected for potential confounding effects of age, sex, education, and APOE status.
Abbreviations: Aβ42/40, plasma amyloid-β 42/40 ratio; FAt, free-water-corrected fractional anisotropy; FW, free-water; GFAP, glial fibrillary acidic protein; GM, gray matter; NfL, neurofilament light; p-tau181, phosphorylated tau 181; t-tau, total tau; WM, white matter.
Significant partial correlations ($p_{FDR} < 0.05$) are denoted using bold font and asterisks(*).

status.[28,30] The current findings indicate that FW changes to hippocampus, basal forebrain, temporal cortex, and transcallosal WM are also sensitive to early deviations in plasma Aβ42/40 and relate to differences in Aβ biological status.

Another key finding was the U-shaped pattern in GM and WM FAt, with reduced FAt in the plasma+/PET- group compared to both plasma-/PET- and plasma+/PET+ groups. Using a different method for FW partial volume correction, a similar pattern was recently reported for cortical GM mean diffusivity in cognitively normal individuals with CSF Aβ42 positive/p-tau negative status compared to individuals with concordant negative and concordant positive CSF Aβ42/p-tau status.[49] One possible explanation for our finding is that increased tissue atrophy in the plasma+/PET+ group allows for more FW to diffuse within interstitial spaces, where reactive astrocytes assemble around the injury site and can lead to an increase in tissue anisotropy.[16,24,50] This explanation conforms to the widespread reduction in cortical volume and thickness measures, as well as the increase in neuronal degeneration (NfL)[51] and neuroinflammation (GFAP)[52] biomarkers in the plasma+/PET+ group.

The correlation analysis between composite imaging scores and plasma biomarkers provides insight into the pathological mechanisms driving the increase in total brain FW. Composite FW scores in both GM and WM were comparable between the plasma+/PET- and plasma+/PET+ groups and did not correlate with Aβ PET Centiloid units. This indicates that the increase in total brain FW was not directly related to total brain Aβ or Aβ PET status. Composite FW scores in both GM and WM yielded an inverse correlation with plasma Aβ42/40 and a positive correlation with p-tau181. Plasma Aβ42/40 ratios were comparable between plasma+/PET- and plasma+/PET+ groups, which is consistent with the finding that plasma Aβ42/40 reaches a plateau early in the AD continuum.[53,54] This may suggest that increasing pathological insult in the brains of plasma+/PET+ individuals, such as tau phosphorylation, could lead to FW exacerbation effects. Concentrations of p-tau181 were increased significantly in the plasma+/PET+ group and correlated positively with GFAP, NfL, and Aβ PET Centiloid units. The increased p-tau181 between plasma+/PET- and plasma+/PET+ stages supports previous findings that p-tau measures associate with increased Aβ pathological load and cognitive diagnosis severity.[53,55–58] The positive correlation between FW and p-tau181 extends findings from previous studies. In brains of AD patients for example, FW correlated positively with ^{18}F-THK5351 PET, which targets tau aggregation and astrogliosis-related neuroinflammation.[59] In another study, regional tau PET SUVRs and FW in entorhinal cortex and parahippocampal gyrus were positively correlated in MCI and AD participants.[33] It is also important to consider the potential contribution of early tau pathology on microstructural decline in the plasma+/PET- group. Although group-level p-tau181 in plasma-/PET- and plasma+/PET- groups did not significantly differ, several participants in both groups had p-tau181 measures that exceeded the positivity cut-point according to healthy normative data in a recent study.[60]

FW imaging has emerged as a clinically relevant tool for tracking progression of neurodegenerative disease. For example, FW is reliably increased in substantia nigra over a 1-year period in patients with Parkinson's disease and predicts subsequent progression of motor and cognitive impairment.[15,16,61–63] The results from this study provide cross-sectional insight into brain microstructure effects that associate with early biological indicators of AD, such as isolated plasma Aβ42/40 positivity, and how FW relates to plasma biomarkers at different biological stages of disease severity. FW imaging may have utility in predicting and monitoring the conversion from Aβ PET negative to positive or future cognitive decline. However, it is important to recognize that not all plasma+/PET- individuals studied here (Aβ42/40 < 0.160) will become Aβ PET positive or progress to dementia over time. In

the study by Schindler et al.,[4] for example, only 7 of 23 Aβ PET negative participants with a positive baseline plasma Aβ42/40 test (Aβ42/40 < 0.1218) converted to Aβ PET positive during the 5.2 ± 2.1 year follow-up period. Plasma Aβ42/40 positive participants, however, were at significantly increased risk for conversion compared to those with concordant negative plasma Aβ42/40 and Aβ PET measures. It is also important to consider the possibility that NC and MCI participants with a negative plasma Aβ42/40 test could develop abnormal Aβ biomarkers or experience future cognitive decline. In the study by Hanon et al.,[13] 18% of MCI participants in the highest plasma Aβ42/40 quartile (Aβ42/40 > 0.169) converted to dementia (95% AD) within 3 years. Large-sample longitudinal assessments are needed to determine the imaging measures and ROIs that hold most promise for early in vivo clinical detection of AD and predicting progression.

This study has several limitations. One consideration is the method for determining plasma Aβ42/40 status and separating Aβ PET negative subgroups (i.e., plasma+/PET- < 0.160 ≤ plasma-/PET-). Despite high overall agreement between plasma Aβ42/40 and Aβ PET status in this study and others (AUC range: 0.8–0.9),[3–5,8] the determined cut-point for plasma Aβ42/40 positivity is variable and subject to differences in sample size and biomarker characteristics. There is a continued need to develop reliable thresholds for plasma Aβ42/40 "positivity," which will better enable cross-study comparisons. Second, Aβ PET status was determined by visual inspection, leading to a relatively higher reference standard for defining PET positivity compared to using PET Centiloid units.[8,64] Third, this study does not rule out secondary pathological causes of brain microstructure decline and cognitive impairment, particularly in the plasma+/PET- group. The data from this study support the position that FW imaging distinguishes groups with positive and negative plasma Aβ42/40, independent of significant group differences in cognitive status, cognitive performance measures, Aβ PET status/Centiloid/SUVR, and other plasma biomarkers (i.e., t-tau, p-tau181, GFAP, NfL). Future studies may include additional biomarkers and be better powered to decompose AD and non-AD pathological underpinnings of microstructure and cognitive decline in plasma+/PET- individuals. A final consideration is that this study lacks longitudinal assessment of imaging and biological disease severity, which will be important for demonstrating the reliability and potential clinical utility of FW imaging.

In conclusion, plasma Aβ42/40 positivity in participants without dementia associates with FW and FAt abnormalities in widespread GM regions and WM tracts. This represents a novel finding that FW imaging is sensitive to early stages of brain microstructure decline, even when brain Aβ reactivity is not adequate to achieve PET positive status. FW effects were exacerbated in the plasma+/PET+ group, whereas a general U-shaped FAt pattern was observed across plasma-/PET-, plasma+/PET-, and plasma+/PET+ groups. We also found that increased brain FW related to worsened plasma Aβ42/40 and p-tau181 measures. With further testing, FW imaging may have clinical utility for monitoring early changes in AD pathophysiology, predicting disease progression, and evaluating therapeutic effects in early-stage trials that recruit participants using high-precision plasma assays.

ACKNOWLEDGMENTS

We thank all research participants and their families from the 1Florida Alzheimer's Disease Research Center for their time and commitment to this research.

This work was supported by the National Institutes of Health [grant numbers: P30AG066506, T32NS082168]. Funding sources were not involved in study design; collection, analysis, and interpretation of data; writing of the report; or in the decision to submit the article for publication.

CONFLICT OF INTEREST STATEMENT

The authors report no relevant conflicts or competing interests. Author disclosures are available in the supporting information.

CONSENT STATEMENT

Participants provided signed consent forms and were in full understanding of study objectives and procedures. All experimental procedures were performed in ethical accordance with the Declaration of Helsinki and were approved and monitored by the local Institutional Review Boards.

ORCID

Jesse C. DeSimone https://orcid.org/0000-0002-3823-8765

REFERENCES

1. Jack CR, Knopman DS, Jagust WJ, et al. Tracking pathophysiological processes in Alzheimer's disease: an updated hypothetical model of dynamic biomarkers. *Lancet Neurol*. 2013;12:207-216. doi:10.1016/S1474-4422(12)70291-0
2. Sperling RA, Aisen PS, Beckett LA, et al. Toward defining the preclinical stages of Alzheimer's disease: recommendations from the National Institute on Aging-Alzheimer's Association workgroups on diagnostic guidelines for Alzheimer's disease. *Alzheimers Dement J Alzheimers Assoc*. 2011;7:280-292. doi:10.1016/j.jalz.2011.03.003
3. Li Y, Schindler SE, Bollinger JG, et al. Validation of Plasma Amyloid-β 42/40 for detecting Alzheimer disease amyloid plaques. *Neurology*. 2022;98:e688-e699. doi:10.1212/WNL.0000000000013211
4. Schindler SE, Bollinger JG, Ovod V, et al. High-precision plasma β-amyloid 42/40 predicts current and future brain amyloidosis. *Neurology*. 2019;93:e1647-e1659. doi:10.1212/WNL.0000000000008081
5. West T, Kirmess KM, Meyer MR, et al. A blood-based diagnostic test incorporating plasma Aβ42/40 ratio, ApoE proteotype, and age accurately identifies brain amyloid status: findings from a multi cohort validity analysis. *Mol Neurodegener*. 2021;16:30. doi:10.1186/s13024-021-00451-6
6. Janelidze S, Teunissen CE, Zetterberg H, et al. Head-to-head comparison of 8 plasma amyloid-β 42/40 assays in Alzheimer disease. *JAMA Neurol*. 2021;78:1375. doi:10.1001/jamaneurol.2021.3180
7. Allué JA, Pascual-Lucas M, Sarasa L, et al. Clinical utility of an antibody-free LC-MS method to detect brain amyloid deposition in cognitively unimpaired individuals from the screening visit of the A4 Study. *Alzheimers Dement Amst Neth*. 2023;15:e12451. doi:10.1002/dad2.12451
8. Rissman RA, Langford O, Raman R, et al. Plasma Aβ42/Aβ40 and phospho-tau217 concentration ratios increase the accuracy of amyloid PET classification in preclinical Alzheimer's disease. *Alzheimers Dement*. 2023. doi:10.1002/alz.13542

9. Burnham SC, Fandos N, Fowler C, et al. Longitudinal evaluation of the natural history of amyloid-β in plasma and brain. *Brain Commun*. 2020;2:fcaa041. doi:10.1093/braincomms/fcaa041
10. Ovod V, Ramsey KN, Mawuenyega KG, et al. Amyloid β concentrations and stable isotope labeling kinetics of human plasma specific to central nervous system amyloidosis. *Alzheimers Dement J Alzheimers Assoc*. 2017;13:841-849. doi:10.1016/j.jalz.2017.06.2266
11. Fandos N, Pérez-Grijalba V, Pesini P, et al. Plasma amyloid β 42/40 ratios as biomarkers for amyloid β cerebral deposition in cognitively normal individuals. *Alzheimers Dement Amst Neth*. 2017;8:179-187. doi:10.1016/j.dadm.2017.07.004
12. Aschenbrenner AJ, Li Y, Henson RL, et al. Comparison of plasma and CSF biomarkers in predicting cognitive decline. *Ann Clin Transl Neurol*. 2022;9:1739-1751. doi:10.1002/acn3.51670
13. Hanon O, Vidal J-S, Lehmann S, et al. Plasma amyloid beta predicts conversion to dementia in subjects with mild cognitive impairment: the BALTAZAR study. *Alzheimers Dement J Alzheimers Assoc*. 2022;18:2537-2550. doi:10.1002/alz.12613
14. Ofori E, Pasternak O, Planetta PJ, et al. Increased free water in the substantia nigra of Parkinson's disease: a single-site and multi-site study. *Neurobiol Aging*. 2015;36:1097-1104. doi:10.1016/j.neurobiolaging.2014.10.029
15. Burciu RG, Ofori E, Archer DB, et al. Progression marker of Parkinson's disease: a 4-year multi-site imaging study. *Brain*. 2017;140:2183-2192. doi:10.1093/brain/awx146
16. Mitchell T, Wilkes BJ, Archer DB, et al. Advanced diffusion imaging to track progression in Parkinson's disease, multiple system atrophy, and progressive supranuclear palsy. *NeuroImage Clin*. 2022;34:103022. doi:10.1016/j.nicl.2022.103022
17. Pasternak O, Sochen N, Gur Y, Intrator N, Assaf Y. Free water elimination and mapping from diffusion MRI. *Magn Reson Med*. 2009;62:717-730. doi:10.1002/mrm.22055
18. Gur Y, Pasternak O, Sochen N. Fast GL(n)-invariant framework for tensors regularization. *Int J Comput Vis*. 2009;85:211-222. doi:10.1007/s11263-008-0196-7
19. Pasternak O, Westin C-F, Bouix S, et al. Excessive extracellular volume reveals a neurodegenerative pattern in schizophrenia onset. *J Neurosci Off J Soc Neurosci*. 2012;32:17365-17372. doi:10.1523/JNEUROSCI.2904-12.2012
20. Metzler-Baddeley C, O'Sullivan MJ, Bells S, Pasternak O, Jones DK. How and how not to correct for CSF-contamination in diffusion MRI. *NeuroImage*. 2012;59:1394-1403. doi:10.1016/j.neuroimage.2011.08.043
21. Febo M, Perez PD, Ceballos-Diaz C, et al. Diffusion magnetic resonance imaging-derived free water detects neurodegenerative pattern induced by interferon-γ. *Brain Struct Funct*. 2020;225:427-439. doi:10.1007/s00429-019-02017-1
22. Wang Y, Wang Q, Haldar JP, et al. Quantification of increased cellularity during inflammatory demyelination. *Brain*. 2011;134:3590-3601. doi:10.1093/brain/awr307
23. Pasternak O, Westin C-F, Dahlben B, Bouix S, Kubicki M. The extent of diffusion MRI markers of neuroinflammation and white matter deterioration in chronic schizophrenia. *Schizophr Res*. 2015;161:113-138. doi:10.1016/j.schres.2014.07.031
24. Budde MD, Janes L, Gold E, Turtzo LC, Frank JA. The contribution of gliosis to diffusion tensor anisotropy and tractography following traumatic brain injury: validation in the rat using Fourier analysis of stained tissue sections. *Brain*. 2011;134:2248-2260. doi:10.1093/brain/awr161
25. Mayer AR, Ling J, Mannell MV, et al. A prospective diffusion tensor imaging study in mild traumatic brain injury. *Neurology*. 2010;74:643-650. doi:10.1212/WNL.0b013e3181d0ccdd
26. Ofori E, DeKosky ST, Febo M, et al. Free-water imaging of the hippocampus is a sensitive marker of Alzheimer's disease. *NeuroImage Clin*. 2019;24:101985. doi:10.1016/j.nicl.2019.101985
27. Archer DB, Schilling K, Shashikumar N, et al. Leveraging longitudinal diffusion MRI data to quantify differences in white matter microstructural decline in normal and abnormal aging. *Alzheimers Dement Diagn Assess Dis Monit*. 2023;15:e12468. doi:10.1002/dad2.12468
28. Archer DB, Coombes SA, McFarland NR, DeKosky ST, Vaillancourt DE. Development of a transcallosal tractography template and its application to dementia. *NeuroImage*. 2019;200:302-312. doi:10.1016/j.neuroimage.2019.06.065
29. Bergamino M, Walsh RR, Stokes AM. Free-water diffusion tensor imaging improves the accuracy and sensitivity of white matter analysis in Alzheimer's disease. *Sci Rep*. 2021;11:6990. doi:10.1038/s41598-021-86505-7
30. Dumont M, Roy M, Jodoin P-M, et al. Free water in white matter differentiates MCI and AD from control subjects. *Front Aging Neurosci*. 2019;11:270. doi:10.3389/fnagi.2019.00270
31. Archer DB, Moore EE, Shashikumar N, et al. Free-water metrics in medial temporal lobe white matter tract projections relate to longitudinal cognitive decline. *Neurobiol Aging*. 2020;94:15-23. doi:10.1016/j.neurobiolaging.2020.05.001
32. Chu WT, Wang W, Zaborszky L, et al. Association of cognitive impairment with free water in the nucleus basalis of meynert and locus coeruleus to transentorhinal cortex tract. *Neurology*. 2022;98:e700-e710. doi:10.1212/WNL.0000000000013206
33. Wang W, Chen R, Mayrand RP, et al. Association of longitudinal cognitive decline with diffusion MRI in gray matter, amyloid, and tau deposition. *Neurobiol Aging*. 2023;121:166-178. doi:10.1016/j.neurobiolaging.2022.10.013
34. Duara R, Loewenstein DA, Greig M, et al. Reliability and validity of an algorithm for the diagnosis of normal cognition, mild cognitive impairment, and dementia: implications for multicenter research studies. *Am J Geriatr Psychiatry Off J Am Assoc Geriatr Psychiatry*. 2010;18:363-370. doi:10.1097/jgp.0b013e3181c534a0
35. Morris JC. The Clinical dementia rating (CDR): current version and scoring rules. *Neurology*. 1993;43:2412-2414. doi:10.1212/wnl.43.11.2412-a
36. Benedict RHB, Schretlen D, Groninger L, Brandt J. Hopkins Verbal Learning Test – revised: normative data and analysis of inter-form and test-retest reliability. *Clin Neuropsychol*. 1998;12:43-55. doi:10.1076/clin.12.1.43.1726
37. Weintraub S, Besser L, Dodge HH, et al. Version 3 of the Alzheimer Disease Centers' Neuropsychological Test Battery in the Uniform Data Set (UDS). *Alzheimer Dis Assoc Disord*. 2018;32:10-17. doi:10.1097/WAD.0000000000000223
38. Weber DM, Kim JC, Goldman S, Racke MK, Clarke NJ. A new LC-MS/MS assay for the quantification of Aβ40 and Aβ42 in plasma: validation and clinical performance. *Alzheimers Dement*. 2022;18. doi:10.1002/alz.064182
39. Wilson DH, Rissin DM, Kan CW, et al. The Simoa HD-1 Analyzer: a novel fully automated digital immunoassay analyzer with single-molecule sensitivity and multiplexing. *SLAS Technol*. 2016;21:533-547. doi:10.1177/2211068215589580
40. Duara R, Loewenstein DA, Lizarraga G, et al. Effect of age, ethnicity, sex, cognitive status and APOE genotype on amyloid load and the threshold for amyloid positivity. *NeuroImage Clin*. 2019;22:101800. doi:10.1016/j.nicl.2019.101800
41. Loewenstein DA, Curiel RE, DeKosky S, et al. Utilizing semantic intrusions to identify amyloid positivity in mild cognitive impairment. *Neurology*. 2018;91:e976-e984. doi:10.1212/WNL.0000000000006128
42. Klunk WE, Koeppe RA, Price JC, et al. The Centiloid Project: standardizing quantitative amyloid plaque estimation by PET. *Alzheimers Dement*. 2015;11:1-15. e1-4 doi:10.1016/j.jalz.2014.07.003
43. Ruopp MD, Perkins NJ, Whitcomb BW, Schisterman EF. Youden Index and optimal cut-point estimated from observations affected by a

lower limit of detection. *Biom J*. 2008;50:419-430. doi:10.1002/bimj.200710415

44. Desikan RS, Ségonne F, Fischl B, et al. An automated labeling system for subdividing the human cerebral cortex on MRI scans into gyral based regions of interest. *NeuroImage*. 2006;31:968-980. doi:10.1016/j.neuroimage.2006.01.021
45. Buckner RL, Head D, Parker J, et al. A unified approach for morphometric and functional data analysis in young, old, and demented adults using automated atlas-based head size normalization: reliability and validation against manual measurement of total intracranial volume. *NeuroImage*. 2004;23:724-738. doi:10.1016/j.neuroimage.2004.06.018
46. Schwarz CG, Gunter JL, Ward CP, et al. [P2–415]: The Mayo clinic adult lifespan template: better quantification across the lifespan. *Alzheimers Dement*. 2017;13. doi:10.1016/j.jalz.2017.06.1071
47. Zaborszky L, Hoemke L, Mohlberg H, Schleicher A, Amunts K, Zilles K. Stereotaxic probabilistic maps of the magnocellular cell groups in human basal forebrain. *NeuroImage*. 2008;42:1127-1141. doi:10.1016/j.neuroimage.2008.05.055
48. Schumacher J, Gunter JL, Przybelski SA, et al. Dementia with Lewy bodies: association of Alzheimer pathology with functional connectivity networks. *Brain*. 2021;144:3212-3225. doi:10.1093/brain/awab218
49. Montal V, Vilaplana E, Alcolea D, et al. Cortical microstructural changes along the Alzheimer's disease continuum. *Alzheimers Dement*. 2018;14:340-351. doi:10.1016/j.jalz.2017.09.013
50. Chad JA, Pasternak O, Salat DH, Chen JJ. Re-examining age-related differences in white matter microstructure with free-water corrected diffusion tensor imaging. *Neurobiol Aging*. 2018;71:161-170. doi:10.1016/j.neurobiolaging.2018.07.018
51. Khalil M, Teunissen CE, Otto M, et al. Neurofilaments as biomarkers in neurological disorders. *Nat Rev Neurol*. 2018;14:577-589. doi:10.1038/s41582-018-0058-z
52. Osborn LM, Kamphuis W, Wadman WJ, Hol EM. Astrogliosis: an integral player in the pathogenesis of Alzheimer's disease. *Prog Neurobiol*. 2016;144:121-141. doi:10.1016/j.pneurobio.2016.01.001
53. Ashton NJ, Janelidze S, Mattsson-Carlgren N, et al. Differential roles of Aβ42/40, p-tau231 and p-tau217 for Alzheimer's trial selection and disease monitoring. *Nat Med*. 2022;28:2555-2562. doi:10.1038/s41591-022-02074-w
54. Chatterjee P, Pedrini S, Doecke JD, et al. Plasma Aβ42/40 ratio, p-tau181, GFAP, and NfL across the Alzheimer's disease continuum: a cross-sectional and longitudinal study in the AIBL cohort. *Alzheimers Dement*. 2023;19:1117-1134. doi:10.1002/alz.12724
55. Karikari TK, Pascoal TA, Ashton NJ, et al. Blood phosphorylated tau 181 as a biomarker for Alzheimer's disease: a diagnostic performance and prediction modelling study using data from four prospective cohorts. *Lancet Neurol*. 2020;19:422-433. doi:10.1016/S1474-4422(20)30071-5
56. Jack CR, Wiste HJ, Algeciras-Schimnich A, et al. Predicting amyloid PET and tau PET stages with plasma biomarkers. *Brain*. 2023;146:2029-2044. doi:10.1093/brain/awad042
57. Milà-Alomà M, Ashton NJ, Shekari M, et al. Plasma p-tau231 and p-tau217 as state markers of amyloid-β pathology in preclinical Alzheimer's disease. *Nat Med*. 2022. doi:10.1038/s41591-022-01925-w
58. Shen Y, Yu W-B, Shen B, et al. Propagated α-synucleinopathy recapitulates REM sleep behaviour disorder followed by parkinsonian phenotypes in mice. *Brain*. 2020;143:3374-3392. doi:10.1093/brain/awaa283
59. Nakaya M, Sato N, Matsuda H, et al. Free water derived by multi-shell diffusion MRI reflects tau/neuroinflammatory pathology in Alzheimer's disease. *Alzheimers Dement Transl Res Clin Interv*. 2022;8. doi:10.1002/trc2.12356
60. Cogswell PM, Lundt ES, Therneau TM, et al. Modeling the temporal evolution of plasma p-tau in relation to amyloid beta and tau PET. *Alzheimers Dement*. 2023. doi:10.1002/alz.13539
61. Ofori E, Pasternak O, Planetta PJ, et al. Longitudinal changes in free-water within the substantia nigra of Parkinson's disease. *Brain*. 2015;138:2322-2331. doi:10.1093/brain/awv136
62. Arpin DJ, Mitchell T, Archer DB, et al. Diffusion magnetic resonance imaging detects progression in PARKINSON'S disease: a placebo-controlled trial of rasagiline. *Mov Disord*. 2022;37:325-333. doi:10.1002/mds.28838
63. Planetta PJ, Ofori E, Pasternak O, et al. Free-water imaging in Parkinson's disease and atypical parkinsonism. *Brain*. 2016;139:495-508. doi:10.1093/brain/awv361
64. Amadoru S, Doré V, McLean CA, et al. Comparison of amyloid PET measured in Centiloid units with neuropathological findings in Alzheimer's disease. *Alzheimers Res Ther*. 2020;12:22. doi:10.1186/s13195-020-00587-5

SUPPORTING INFORMATION

Additional supporting information can be found online in the Supporting Information section at the end of this article.

How to cite this article: DeSimone JC, Wang W-E, Loewenstein DA, et al. Diffusion MRI relates to plasma Aβ42/40 in PET negative participants without dementia. *Alzheimer's Dement*. 2024;1-13. https://doi.org/10.1002/alz.13693